# The Effect of Shot Peening on Notched Low Cycle Fatigue

**K. A. Soady[1,*], B. G. Mellor[1.], J. Shackleton[2.], A. Morris[3.], P. A. S. Reed[1.]**

1. School of Engineering Sciences, University of Southampton, SO17 1BJ, UK
2. Materials Science Centre, University of Manchester, M1 7HS, UK
3. E.ON New Build and Technology Ltd., Technology Centre, Ratcliffe on Soar, Nottingham, NG11 0EE, UK

***Corresponding Author: K.A.Soady@soton.ac.uk; +44 (0) 2380 599450**

## Abstract

The improvement in low cycle fatigue life created by shot peening ferritic heat resistant steel was investigated in components of varying geometries based on those found in conventional power station steam turbine blades. It was found that the shape of the component did not affect the efficacy of the shot peening process, which was found to be beneficial even under the high stress amplitude three point bend loads applied. Furthermore, by varying the shot peening process parameters and considering fatigue life it has been shown that the three surface effects of shot peening; roughening, strain hardening and the generation of a compressive residual stress field must be included in remnant life models as physically separate entities. The compressive residual stress field during plane bending low cycle fatigue has been experimentally determined using X-ray diffraction at varying life fractions and found to be retained in a direction parallel to that of loading and to only relax to 80% of its original magnitude in a direction orthogonal to loading. This result, which contributes to the retention of fatigue life improvement in low cycle fatigue conditions, has been discussed in light of the specific stress distribution applied to the components. The ultimate aim of the research is to apply these results in a life assessment methodology which can be used to justify a reduction in the length of scheduled plant overhauls. This will result in significant cost savings for the generating utility.

## Keywords

Low cycle fatigue, stress concentration, shot peening, residual stresses, ferritic heat resisting steel

## Nomenclature

$R_a$ Surface roughness; the arithmetic mean of the absolute values of the vertical deviations of the roughness profile from the mean line (μm)

| | |
|---|---|
| $s$ | Load span (mm) |
| $R$ | Load ratio |
| $\varepsilon$ | True strain |
| $\sigma$ | True stress (MPa) |
| $E$ | Elastic modulus (GPa) |
| $\sigma_y$ | Yield stress (MPa) |
| $A$, $n_m$ | Monotonic Ramberg-Osgood model coefficients |
| $v$ | Poisson's ratio |
| $\sigma_\varphi$ | Single stress acting in a chosen direction $\varphi$ (MPa) |
| $\varphi$ | Angle between a fixed direction in the plane of the sample and the projection in that plane of the normal to the diffracting plane (°) |
| $\psi$ | Angle between the sample normal and the diffracting plane normal (°) |
| $d_{\varphi\psi}$ | Interplanar spacing of strained material in direction of measurement defined by $\varphi$ and $\psi$ |
| $\theta$ | Angle between incident ray and scattering atomic plane (°) |
| $H_v$ | Vickers Hardness |
| $\sigma_{0.2}$ | 0.2 % proof stress (MPa) |
| $\sigma_{uts}$ | Ultimate tensile strength (MPa) |
| $\Delta\varepsilon$ | Strain range |
| $N_f$ | Number of cycles to failure |
| $R_q$ | Surface roughness; the root mean square of the absolute values of the vertical deviations of the roughness profile from the mean line (μm) |

# Abbreviations

| | |
|---|---|
| LCF | Low Cycle Fatigue |
| NDT | Non-Destructive Testing |
| HCF | High Cycle Fatigue |
| EDM | Electrical Discharge Machining |
| LP | Low Pressure |
| XRD | X-Ray Diffraction |
| EBSD | Electron Back Scattered Diffraction |

# 1. Introduction

Within conventional power stations, steam turbine components are safety critical parts which are subjected to low cycle fatigue (LCF) stresses of thermal and mechanical origin during start up and shut down. Non-destructive testing (NDT) is carried out during routine maintenance inspections (approximately every 12 years) to locate and size any defects, especially at the fir tree blade-disc interfaces which contain several severe stress concentrations. A range of refurbishment activities are then undertaken to ensure the performance and integrity of the turbine rotor during the next operational cycle. Typically, a major outage on a conventional power station takes 8 – 12 weeks. For a large 500MW unit the cost in lost generation over this period is substantial (>£M); as a result there is a drive to minimise the scope of remedial works undertaken allowing the length of the outage to be reduced. Hence, there is a great need to develop life assessment methods that can be used to justify deferring invasive inspections and reducing the scope of the maintenance works.

A damage tolerant fatigue lifing approach is used to determine the maximum number of future start up and shut down operations and allow component repair and replacement scheduling. Many UK operational turbines are of 1960s vintage and have undergone ~3500 start up / shut downs already; these ageing assets must be repaired or replaced in the most cost effective manner whilst maintaining safety margins.

Power plant steam turbine blades are most commonly manufactured from ferritic heat resistant steels (9-12%Cr-Mo-V)[1]. These are fully tempered martensitic steels characterised by well formed laths and a high dislocation density of the order $10^{14}$ $m^{-2}$ [2]. Relatively large $Cr_{23}C_6$ particles are present at grain and subgrain boundaries and finer MX [(V,Nb)(C,N)] and $M_2X$ [$(Mo,Cr,V)_2(C)$] precipitation hardening dispersoids are found within grains and sub-grains after tempering [3].

Shot peening is a cold work process applied to blade regions of stress concentration (such as the blade-disc interface) in an attempt to reduce the susceptibility of this geometrically complex region to fatigue. The overall beneficial effect of shot peening on high cycle fatigue (HCF) resistance is widely recognised [4].

The effect of the shot peening process on LCF is not as well understood, and as a result, it is not currently implemented in life assessment models for components operating in this regime but considered to be an additional safety factor that results in conservative lifing. The

inclusion of this process may enable the extension of remnant life estimates resulting in significant cost savings to power station operators.

The component surface is bombarded with small spherical shots of a hard material, usually hardened cast steel, at a relatively high velocity (40 – 70 $ms^{-1}$) [5]. The surface is roughened by intense local plastic deformation; the altered zone size has been reported to be approximately 20-30 μm (an order of magnitude greater than the plastically deformed region resulting from milling)[6]. This localised plastic deformation also results in strain hardening which increases the yield strength of the material near the surface. The plastic strain decreases with depth until at a certain depth only elastic deformation has occurred. At the release of contact this elastic region tends to recover to the unloaded state; the plastically deformed region consequently sustains some permanent deformation. The continuity condition requires the development of a compressive residual stress field (of typical depth 50 – 500 μm) parallel to the free surface; a balancing tensile residual stress beneath this maintains force equilibrium in the component [7, 8]. The magnitude and depth of the compressive residual stress field has been shown to be dependent on the peening process parameters [9] and target material [10].

Surface roughening is generally considered detrimental in terms of fatigue life (due to the presence of micro stress concentrators and accelerated crack initiation) [11, 12]. The beneficial effect of shot peening is a result of coupling of the residual stresses and strain hardening [7] although the relative beneficial contributions of each are still controversial [13]. It has been reported that the beneficial effect of strain hardening is in increasing the initiation life since high dislocation densities in the cold worked region result in higher yield stresses [7, 14] and thus lower plastic strain amplitudes under stress controlled cycling [15]; any reduction in crack propagation life caused by the low residual ductility of the strain hardened region is less significant than the increase in initiation life [7]. The presence of compressive residual stresses can increase both initiation and crack propagation lives as a result of a reduction in the effective applied tensile stress[13].

Stresses in LCF reach levels sufficient for plastic deformation and corresponding residual stress relaxation. When the residual stresses combine with the applied stresses to cause local plastic yielding, the plastic misfit is reduced and the residual stress profile is modified. Residual stress relaxation can occur when either tensile or compressive (eg. during unloading) stresses in excess of the yield strength are effectively applied to the component.

The summation of residual stresses with applied stresses means that the magnitude of applied compressive stresses required to cause local yielding and initiate relaxation is less than the required magnitude of applied tensile stresses [16]. This effect is enhanced by the Bauschinger effect which reduces the compressive yield strength after initial tensile cold work (which was required to generate the compressive residual stresses). Analytical models incorporating the Bauschinger effect have been developed for this relaxation [16, 17].

The degree of relaxation is heavily dependent on the component geometry, specific loading mechanism (the applied cyclic stress distribution) and material characteristics of a particular shot peened system (for example yield strength, cyclic softening characteristics and the modification of these by the intense cold work in the near surface layer [17]).

Several investigations into the relaxation of compressive residual stress profiles after fatigue cycling are reported in the literature; indeed a recent review [18] reports over 65 articles which address the cyclic stability of peening residual stresses. It is noted, however, that the majority of this work considers the relaxation of such residual stresses in flat, axially loaded samples. In this case, the maximum relaxation occurs in the longitudinal direction compared to the transverse direction; with the most significant load dependent relaxation occurring after one cycle [19]. Where more geometrically complex samples are experimentally considered, they are axially loaded [20] and where other loading conditions are considered, the samples are not geometrically complex [10, 21].

More recently, the relaxation of residual stresses has been considered in a 12Cr low pressure steam turbine blade steel [22]. However, the samples were flat and axially loaded to stresses in excess of yield with $R > 0.9$ so it is thought that the authors were replicating the HCF conditions experienced under normal operating conditions. Nonetheless, relaxation in residual stress is reported in the loading direction when the mean stress is equal to the yield stress of the material. After the initial cycle, the reduction in residual stress is shown to follow a log-linear trend; this continued relaxation is highly dependent on the cyclic stress-strain characteristics of the material in question.

The overall objective of this work is to quantify the effect of shot peening on large amplitude low cycle fatigue in notched components. Firstly, the effect of shot peening on samples of differing notch geometry is quantified in terms of surface roughness and total life as a means of determining whether the shape of a component affects the efficacy of the shot peening process.

Secondly the requirement of separating the beneficial effects of strain hardening and compressive residual stresses when including the effects of shot peening in life estimates is clarified. This is achieved through presentation of fatigue life data for notched components subjected to differing shot peening processes and comparison of this data with that taken from samples ground to a power generation industry specification. This work acts as justification for the third experimental phase; the analysis of residual stress depth profiles in shot peened notched samples loaded in three point bend.

The authors believe this work is novel in that the relaxation of shot peening residual stresses in notched components is experimentally considered in the light of the consequential effect on total fatigue life. Rather than axially loading samples, they have been loaded under large amplitude three point bend; these conditions more accurately represent the service loading conditions of fir tree blade connectors than the axially loaded geometrically flat samples which have been previously studied relatively extensively. Indeed, to the best of the authors' knowledge, experimental data relating to neither the effect of shot peening on total LCF life in this material system nor the extent of residual stress relaxation under bend load in notched components have been reported previously. The improved understanding of the effect on fatigue life will enable better exploitation of shot peening technology in this application in the future.

# 2. Experimental Methods

## 2.1. Material and Sample Preparation

All testing has been carried out on FV448, which is a 9-12Cr-1Mo-V steel representative of those which are typically applied in low pressure turbine blades. The nominal composition and the results of a spectrographic analysis are detailed in Table 1. This material is typically austenitised at 1150 °C, oil quenched and tempered at 650 °C [23] resulting in a tempered martensitic microstructure. The specific mechanical properties were determined by hardness testing (in accordance with BS EN ISO 6507-1:2005 [24]) and tensile testing (in accordance with BS EN 10002-1:2001 [25]).

All sample notches were manufactured with circular profile notch geometries defined by their depth and diameter. In order to remove any artefacts resulting from the prior machining of samples by electrical discharge machining (EDM), 0.25 mm was removed from the surface

by a grinding process, so that the surface roughness met the industrial machined component (and pre-peen) specification of $R_a$ < 0.8 μm. The roughness of the surface, $R_a$, was determined for all samples at several locations around the notch using a Taylor Hobson Form Talysurf 120L stylus profilometer in accordance with BS EN ISO 4287:2000 [27]; the profile filter was selected in accordance with BS ISO 4288:1996 [28].

To simulate the effect of varying component geometry on the efficacy of the shot peening process, notch geometry was varied in accordance with Table 2 (all samples had total width in the direction of crack growth 7.75 mm and breadth 8.00 mm). The shot peening process used was that employed during the peening of turbine blade components, namely MI230R, 13A, 200%, carried out by Metal Improvement Company, Derby Division.

To investigate the effect of varying the shot peening process parameters, the blade connection simulation geometry was used. The effect of varying intensity was considered by using three shot peening processes of varying intensity (4A, 13A, 18A). The effect of the means of achieving a given intensity by varying shot diameter and velocity was considered by using two shot peening processes at the same intensity (13A). The various shot peening processes used are detailed in Table 3 and identified by T0-3.

## 2.2.Low Cycle Fatigue Conditions

The maximum service temperature in low pressure (LP) turbines of 250 °C is outside the creep regime for this material and is not thought to have a significant effect on fatigue life. As a result room temperature fatigue testing with a sinusoidal waveform and frequency 20 Hz has been carried out using a servo hydraulic Instron 8502. The samples were loaded in three point bend with load span, $s$ = 15 mm. Although the tests were carried out in load control with $R$ = 0.1, an elastic plastic finite element model was developed using data taken from monotonic tensile testing (allowing isotropic hardening) to simulate the true stress and strain ranges experienced at the notch root. At the relatively high stresses and strains under present consideration, the material could be equally well represented (<2% error) by a simple material model which uses the 0.2% proof stress as the limit of proportionality and the direct input of data inputs in the plastic region or by a Ramberg Osgood model (Equation 1); however the Ramberg Osgood model is considered generally more satisfactory as it provides a better representation of material behaviour in the yield region.

$$\varepsilon = \frac{\sigma}{E} + \left(\frac{\sigma}{A}\right)^{\frac{1}{n_m}}$$

(1)

The relevant materials model parameters are given in Table 4. In order to capture the stress gradient of interest at the notch root elements (of 20 node quadratic brick, full integration type) adjacent to the surface were 0.01 mm in depth; this value gradually increased to 0.1 mm over a depth of 1 mm. It was consideration of the local true strain range at the centre of the notch that defined the testing loads; to this end, the model was also used to determine the stress and strain distribution through the samples under sequential maximum, minimum and zero static loads.

## 2.3.X-Ray Diffraction to Measure Residual Stresses

The most common experimental method for determining shot peening residual stress profiles is laboratory X-Ray Diffraction (XRD) and incremental layer removal by electropolishing. It offers better spatial and depth resolution than mechanical methods [29] and is preferred to non-linear ultrasonic, magnetic and electrical methods because of the requirement of stress free samples and errors introduced by grain size, preferred orientation and cold work for these techniques [30]. Not only does XRD reduce these errors, but it is able to differentiate between the macrostresses and the microstresses which result from strains over distances of the order of or less than crystal dimensions and which are introduced, for example, by cold work [29]. The most common technique, and that employed in the present investigation, for determining residual macrostresses is the $\sin^2\psi$ method; the theoretical derivation of this is well described elsewhere [31, 32] and as such is not considered here. The residual stress present can be determined through application of Equation 2 without the requirement of a stress free reference.

$$\sigma_\phi = \left(\frac{E}{1+\upsilon}\right)\left(\frac{1}{d_{\phi 0}}\right)\left(\frac{\partial d_{\phi\psi}}{\partial \sin^2\psi}\right)$$

(2)

Data was collected at the base of the notch for three notched samples (4.5 x 1.25 mm notches) in each surface condition (ground / shot peened T0) which were each at a different total life fraction (uncycled, one cycle and estimated 50% total life). This data was collected in the two orthogonal directions illustrated in Figure 1. Data was also obtained for one flat shot peened sample in the uncycled condition.

Measurements were made using a Proto iXRD device and incremental layer removal was achieved by an electropolishing method. The electrolyte was 8% (by volume) of 60% perchloric acid solution mixed in solution with 92% (by volume) of glacial acetic acid. Near the surface, depth increments were approximately 30 μm; once the maximum residual stress had been recorded, the increments were increased to a maximum of approximately 100 μm at the greatest depths.

A Cr-Kα X-ray source was used with a wavelength of 2.291 Å and measurements were taken on the {211} diffraction peak which was recorded at a $2\theta$ angle of approximately 156 °. The diffraction elastic constant was $5.92 \times 10^{-6}$ $MPa^{-1}$. In order to minimise error associated with taking residual stress measurements on a curved surface, the smallest collimator available (0.5 mm diameter) was used. The X-ray penetration depth in ferrite was estimated using data taken from the literature [32] for Cr radiation on the {211} peak at $\psi = 0°$ (ie. where penetration is at its greatest) to be 5 μm. The irradiated area was less than 0.4 times the radius of curvature of the analysed surface in the direction of the stress component [31]. At the beginning of each working day a 'gain' or flat field correction was carried out to account for the variation in efficiency across the 512 positions on each detector and between the two detectors. The profile was corrected by dividing the peak by gain.

When the beam was rotating in the axial direction, there were no notch shadowing effects, and thus fourteen $\psi$ angles varying from -39 to +39 ° were considered across two detectors. When the beam was rotating in the radial direction however, notch shadowing effects became more significant and the fourteen $\psi$ angles measured only ranged from -30 to +30°.

# 3. Results and Discussion

## 3.1. Material Characterisation and Surface Treatment Effects

FV448 has a tempered martensite microstructure; the specific mechanical properties and material model details are given in Table 4.

The surface microhardness profiles after grinding (before shot peening) and after shot peening are illustrated in Figure 2. Whilst the grinding process has had no significant effect on the near-surface micro hardness when compared with the bulk mean, it is clear that the apparent hardness has increased as a result of the shot peening process. Figure 3 shows the corresponding microstructures as revealed by Vilella's reagent; there is no apparent phase

change after either the grinding or shot peening process over the length scale illustrated. Grain refinement over the first 70 μm is, however, apparent after the shot peening process.

It was found that there was no significant variation in surface roughness either at varying locations around each notch or between different notch geometries using a paired t-test with p-value < 0.05. The surface roughness resulting from the MI230R 13A 200% process was $R_a$ = 3.39 ± 1.06 μm. These results are illustrated graphically for the blade-disc interface simulation geometry in Figure 4. Indeed where we might have expected the surface roughness inside the notch to reduce with notch shadowing effects preventing shot impingement, in fact the mean $R_a$ around the notch was higher than the mean $R_a$ on the flat surfaces. This indicated that the process used was sufficient to peen all areas of the sample.

The effect of varying the shot peening process parameters on the surface roughness is detailed in Table 5.

## 3.2.Low Cycle Fatigue

Figure 5 shows total life data (in terms of true strain ranges at the centre of the notch in the loading direction) for samples with different notch geometry. The data is shown using a Coffin-Manson type approach as although the material is yielded under the first cycle in tension, the compressive load is not sufficient to exceed yield in the compressive direction; hence total strain amplitude is shown on the vertical axis. Wider notches appear to have a lower fatigue life; this is not, however, considered to be a result of variations in the efficacy of the shot peening process (if the effect was due to notch shadowing, we would expect the lower life in the most severe 4.5 x 3 mm notch) but a result of the high tensile stresses resulting from bending extending to greater depths below wider notches (Figure 6). Indeed these elevated stresses extend to a depth beyond that which the residual stresses from the shot peening process may be expected to act; the larger sampling volume at elevated stress increases the probability of fatigue initiation.

The effect of varying the intensity of the shot peening process is shown in Figure 7. The low intensity (4A) process offers very little improvement in total life over that of the ground samples in LCF conditions. Increasing the intensity from 13A to 18A has resulted in no improvement in total life even though the compressive residual stress profiles would be expected to be deeper. This effect may be a result of the higher surface roughness facilitating initiation (Table 5). Using larger shot at a lower velocity to develop the same intensity results

in lower surface roughness but there is a negligible effect on the fatigue life (Figure 7). The amount of strain hardening resulting from the lower velocity impacts may be reduced and in this case the corresponding reduction in initiation life may be affecting total life.

The effect of surface roughness on fatigue life is already well documented [11, 33, 34] and as such is not the focus of this paper, since it has previously been concluded [34] that for roughness values in the range $2.5 < R_a < 5$ μm, workpiece residual stress and surface microstructure dominate. However, roughness is reported in the present study since it has been shown that for stress relieved AISI4140, even low surface roughnesses $R_a = 1.4$ μm had a detrimental effect compared to polished samples at $R_a = 0.3$ μm. In the absence of residual stresses and microstrains, a separate study on AISI304 stainless steel has shown crack initiation time is dependent on $R_q$ according to an equation of form $\propto R_q^{-0.21}$ [35]. Should mechanical residual stress relief be a feature of the specific operating conditions, surface roughness must be considered as a factor affecting initiation life; for damage tolerant models where crack propagation is considered, surface roughness has no effect. Hence the inclusion of surface roughness in the life assessment model is dependent on residual stress relaxation and the modelling approach in use. It is for this reason that the present paper focuses on mechanical stress relief under service replicating conditions.

Figure 7 also illustrates the beneficial effect of applying the industrial shot peening process to pre-ground notched samples even when they are tested in the LCF regime, although the relative magnitude of the beneficial effect is reduced as the number of cycles is reduced. This reduction may be a result of the relaxation of residual stresses; this was another consideration which led to the focus of the present paper on residual stress relaxation.

The true strain range at which the samples used to investigate residual stress relaxation were fatigue cycled was $11.1 \times 10^{-3}$. This was selected because a small increase in strain from $10.5 \times 10^{-3}$ to $11.1 \times 10^{-3}$ has resulted in a significant change in the relative benefit of shot peening (Figure 7).

## 3.3. Residual Stress Profiling

### 3.3.1. Residual Stress Profiles after Shot Peening

Given the equibiaxiality of the shot peening residual stress field when the impinging shot is normal to the surface, significant macro-shear stresses were not expected to be present in the samples [10, 36, 37]. This was confirmed for this specific peening process using the uncycled

flat shot peened sample (Figure 8) and as a result, any $\psi$ splitting detected in the notched samples' radial direction was considered to be a result of notch curvature and an appropriate correction was applied [38].

The error was determined by calculating the sample standard deviation over 5 bi-directional measurements (10 data points) at different locations on the uncycled flat shot peened sample. The standard deviation was 25 MPa; as a result the 95% confidence range was ±50 MPa. Due to time constraints and equipment availability, this was assumed to be the confidence with which all data could be quoted rather than carrying out repeat measurements for each notched sample data point.

Although the samples had a slight curvature, an appropriate analytical depth correction solution was that for a flat plate [39]. It was assumed that the relaxation stress had a linear distribution over the cross section of the remaining material with the same integrated force and moment as the stress in the removed layer but of opposite sign.

Figure 8 shows a comparison of the residual stresses resulting from shot peening in pre-ground notched and flat samples. Given the expected measurement variability, there is no significant difference between the stress distributions in both directions in the flat sample and the stress distribution in the transverse direction in the notched sample; however the stress distribution in the notched sample longitudinal direction appears to be more compressive. The depth to which the elevated compressive stress extends is, however, unchanged with the stress beginning to increase towards zero in all four cases at approximately 200 μm. The total depth of the compressive residual stresses in all cases was 340 μm.

Whilst the increased magnitude of longitudinal compressive residual stress may not have been anticipated in the notch root given the potential shadowing effect of the notch in preventing shot impinging at the base of the notch, these results are in line with previous work [20] and the increased mean $R_a$ found at varying locations around the notch.

The effect of applying fatigue cycles to notched shot peened samples on surface residual stresses is illustrated in Figure 9. In the transverse direction (a) there is a reduction in the residual stress magnitude after the application of fatigue cycles but no change in the overall depth of the compressive stress field and after approximately 250 μm the uncycled shot peened profile is retained. This trend is not shown in the longitudinal direction (b) where the original residual stress profile is retained after fatigue cycling.

The relaxation of post-shot peen residual stresses in the transverse direction is thought to be a direct result of the mechanisms reported by other researchers [16, 19]. Under loading, residual stresses combine with applied stresses to cause local plastic yielding and reduce the plastic misfit which caused the presence of the residual stresses.

The surface stress relaxation to 78 % of its original value can be compared with similar work [10] (in this case, the measurement was taken after 1000 cycles in a material which does show some logarithmic relaxation with increasing cycles) where a flat (aluminium alloy) sample was loaded to a maximum stress greater than yield under four point bend with $R$ = 0.1. In this case the stress relaxed to 82 % of its initial value; this shows good correlation with the present results. However, whilst not explicitly defined, it is assumed that the direction of stress measurement in this work [10] was parallel to the loading direction. In the present work, there is no stress relaxation observed in the longitudinal loading direction.

It has been noted in several works [16, 19] that the relaxation is greatest in the direction parallel to the applied load rather than perpendicular to it. This effect is not apparent in the present investigation. The material near the surface which is yielded in tension develops a compressive residual stress after unloading as a result of constraint by the elastically deformed material beneath. This constraint opposes any relaxation which may occur in the loading phase of the fatigue cycle because the unloading still produces a superposing compressive residual stress. In addition the initial load-induced tensile stress needs to overcome the residual compressive stress from shot peening, and the local effect of work hardening from the shot peening may also be expected to affect the stress distribution.

The residual stress profiles after one cycle and half the samples' expected total life are the same in both the ground and shot peened conditions (Figure 9). This trend indicates that there is minimal logarithmic relaxation in this material. The lack of stress relief in the direction of loading would tend to indicate that under these conditions, surface roughness would continue to have a negligible effect on total life.

### 3.3.2. Residual Stress Profiles after Grinding

Figure 10 illustrates the residual stresses present in notched samples after grinding; comparison with the data already presented in Figure 8 confirms that the industrial shot peening process (T0) is sufficient to remove the pre-peen residual stresses. All grinding took place in the transverse direction; in this direction at the surface no residual stress has been recorded. This is in contrast to the longitudinal direction where there is an apparent surface

compressive residual stress. In both cases the residual stress increases to a maximum tensile stress at approximately 25 μm; the magnitude of this tensile stress is greater in the longitudinal direction. The residual stress then decays to a balancing tensile stress.

The shape of the post-grinding residual stress profile is similar to that which has been reported previously [41]. The 'more tensile' residual stress at the surface in the transverse (grinding) direction would be expected [41-43]; however, the higher maximum tensile residual stress in the longitudinal direction is contrary to previous work [41, 42]. This may be a result of the need to balance the surface compressive residual stress; this change of sign near the surface in the longitudinal direction has also not been reported in other work.

There are three mechanisms of generating residual stresses during grinding: mechanical deformation, thermally induced deformation and phase transformations in hardened steels [42]. One possible explanation for this change in sign is the increased dominance of the mechanical residual stress creation mechanism at the notch surface (stress concentrator) and a resulting compressive residual stress despite the high temperature of the grinding process which has resulted in tensile residual stresses at greater depths.

One other possible explanation would be the attainment of temperatures in excess of that required to form austenite during the grinding process and the formation of untempered martensite at the sample surface with a corresponding compressive residual stress; overtempered material would be present in subsurface layers with a corresponding tensile residual stress. The formation of untempered martensite at the sample surface would be associated with a variation in microhardness. Phase changes were eliminated as the cause of the grinding residual stresses using the data illustrated in Figure 2. There is clearly no significant change in microhardness at the indent closest to the surface (67 μm and so within the region of tensile residual stress illustrated in Figure 10(b)) and that which is furthest from the surface (220 μm). Furthermore, as illustrated in Figure 3(a) there is no apparent variation in microstructure with distance from the ground surface.

After fatigue cycling, in the transverse direction there has been a reduction in the tensile residual stress magnitude; indeed at the surface the residual stresses are now compressive. This effect is even more marked in the longitudinal direction. In both cases, the resulting residual stresses are the same after one cycle and half the expected total life, this indicates that the change in residual stress occurs after the first cycle and provides further evidence supporting the lack of logarithmic stress relaxation through life in this material.

The relaxation of both longitudinal and transverse grinding residual stresses has been reported previously [21, 40, 42]. The generation of the compressive residual stress field in this work supports the conclusion that the initial residual stress profile from machining was relaxed within the first tensile half cycle and from that point onwards at each strain reversal the residual stress changed [40]. In this case the unloading from high tensile stresses has resulted in a compressive residual stress field.

The material near the surface is yielded under tension, and yet the material beneath is not; upon release of the load, the elastically deformed material places the near surface plastically deformed material under compression. The effect is present in both directions. This mechanism is a direct result of the loading under three point bend, and would perhaps not be expected to be so significant (especially in the longitudinal direction) in axially loaded samples where even with the stress concentrating feature the bulk may be expected to deform plastically under maximum load. This mechanism is similar to that which is present in the shot peened samples, however, the residual stresses are of lower magnitude and of shallower depth, indicating that any variations in material properties resulting from strain hardening might also be expected to be less severe. This means the ground sample data is helpful in developing finite element models which can predict residual stress relaxation.

In order to demonstrate this potential, the residual stress present at the notch root in the longitudinal and transverse directions generated by unloading after the application of one stress cycle (in material with no residual stress or variation in material properties) was determined using the finite element model described in Section 3.2. This data has been shown in conjunction with the experimental results on the ground samples in Figure 10. The high bending stresses under maximum load in the longitudinal direction shown in Figure 6 result in a compressive residual stress after load release. The correlation between experimental and computational results is sufficient to add confidence to the experimental data. For this simple case, the method clearly shows potential for modelling the residual stress distributions after loading and it is in developing this approach where future efforts will be focussed.

In Section 3.3.1, the retention of the shot peening residual stress profile was considered to be a result of the combination of the residual stresses present, the loading type and strain hardening. The model in its present state can account for the loading type, but in order to account for the residual stresses and strain hardening, consideration of the material's cyclic stress-strain characteristics must be made. Once this data is available, we intend to use a more

appropriate material model, such as a combined isotropic and kinematic hardening approach, which can capture the material evolutionary behaviour to model firstly the shot peening process (several approaches to this are well documented in the literature, one such physical model which would be appropriate for application in the present work is the multiple impingement model first developed by Meguid [44]) and then the fatigue cycling. This approach would be able to capture both variations in material properties resulting from shot peening and also residual stress development which can be verified against the experimental data reported in the present work before application to complex components. The variation in yield stress through the component resulting from strain hardening will also require verification. It is anticipated that the data reported in Figure 2 will go some way towards allowing this.

A comparison of the micro hardness and residual stress depth profiles in notched samples (as shown in Figure 2 and Figure 8 respectively) is illustrated in Figure 11. Whilst micro hardness can be affected by both residual stresses [45] and strain hardening [10, 19], for the present material where $E/\sigma_y = 250$, the variation in measured hardness caused by a biaxial residual stress field of -0.8 $\sigma_y$ would be expected to be around 5% [46] and thus within experimental error. However, the correlation between microhardness and the magnitude of yield stress in highly work hardened materials is not well defined and a calibration process will be required. In order to improve confidence in the results such that they can be applied in lifing methods, XRD line broadening and electron back scattered diffraction (EBSD) data will also be calibrated to provide indications of the magnitude and depth of influence of strain hardening.

# 4. Conclusions

1. Shot peening notched samples increases the total fatigue life, even when operating in LCF conditions.
2. The notch shape does not affect the efficacy of the shot peening process, but there are intrinsic lifetime effects resulting from increased sampling volume effects in wider notches.
3. The need to separate the beneficial effects of strain hardening and compressive residual stresses from shot peening before including the effects of shot peening in lifing estimates has been established. Where strain hardening and residual stresses are

significant throughout the component life, surface roughness is not considered to be a significant factor in the damage tolerant lifing process.

4. Cyclic plastic deformation of a notched shot peened component under three point bend results in:
    - The retention of any near surface compressive residual stresses (for example resulting from the shot peening process) in the direction of loading and relatively small relaxation in the orthogonal direction (to approximately 80% of the original value)
    - The conversion of near surface tensile residual stresses (for example resulting from a grinding process) to compressive residual stresses in the direction of loading.
5. The lack of relaxation of residual stresses in this constrained geometry may explain the observed continued retention of shot peening benefit, even to LCF.

This data will facilitate the inclusion of the effects of the shot peening process in the damage tolerant life assessment models which are applied to geometrically complex components operating under LCF conditions in power plant; the authors note that further data pertaining to the cold work profile resulting from the shot peening process and its subsequent redistribution with fatigue cycling is also required in improved lifing models; whilst the intended approach has been introduced here, a detailed discussion of this is beyond the scope of the present paper. This will reduce the level of conservatism in the models and will facilitate an improvement in the cost effectiveness of repair and replacement scheduling by extending component life whilst maintaining safety margins.

## Acknowledgements

Financial support from the Engineering and Physical Sciences Research Council, E.ON New Build and Technology Ltd. and The Royal Commission for the Exhibition of 1851 is gratefully acknowledged. The code for generating the FE model produced by Allan Burke-Veliz (formerly of the University of Southampton and now of Tecnologico de Monterrey Campus Toluca) is also gratefully received. Thanks must also be extended to Senzhe Shu, Shaun Ross and Hannah Morton, all students at the University of Southampton, for their assistance in collecting surface roughness, total fatigue life and residual stress data respectively.

## References

[1] F. Masuyama, ISIJ International, 41 (2001) 612 - 625.

[2] K. Maruyama, K. Sawada, J. Koike, ISIJ International, 41 (2001) 641 - 653.

[3] J. Janovec, M. Svoboda, A. Kroupa, A. Výrostková, Journal of Materials Science, 41 (2006) 3425 - 3433.

[4] A.M. Eleiche, M.M. Megahed, N.M. Abd-Allah, Journal of Materials Processing Technology, 113 (2001) 502 - 508.

[5] S.A. Meguid, Finite Elements in Analysis and Design, 31 (1999) 179 - 191.

[6] B. Okolo, F. Pérez-Willard, J. Hawecker, D. Gerthsen, A. Wanner, Journal of Materials Processing Technology, 183 (2007) 160 - 164.

[7] L. Wagner, in: R.R. Boyer, D. Eylon, G. Lutjering (Eds.) Fatigue Behaviour of Titanium Alloys, TMS, Warrendale, PA, 1999, pp. 253 - 265.

[8] D.A. Hills, R.B. Waterhouse, B. Noble, Journal of Strain Analysis, 18 (1983) 95 - 100.

[9] Y. Gao, M. Yao, J. Li, Metallurgical and Materials Transactions A, 33A (2002) 1775 - 1778.

[10] M. Benedetti, T. Bortolamedi, V. Fontanari, F. Frendo, International Journal of Fatigue, 26 (2004) 889 - 897.

[11] J.K. Li, Y. Mei, W. Duo, W. Renzhi, Fatigue and Fracture of Engineering Materials and Structures, 15 (1992) 1271 - 1279.

[12] L. Wagner, Materials Science and Engineering A, A263 (1999) 210 - 216.

[13] M.N. James, D.J. Hughes, Z. Chen, H. Lombard, D.G. Hattingh, D. Asquith, J.R. Yates, P.J. Webster, Engineering Failure Analysis, 14 (2007) 284 - 395.

[14] E.R. De Los Rios, A. Walley, M.T. Milan, G. Hammersley, International Journal of Fatigue, 17 (1995) 493 - 499.

[15] I. Altenberger, B. Scholtes, U. Martin, H. Oettel, Materials Science and Engineering A, 264 (1999) 1 - 16.

[16] H. Holzapfel, V. Schulze, O. Vöhringer, E. Macherauch, Materials Science and Engineering A, A248 (1998) 9 - 18.

[17] W.Z. Zhuang, G.R. Halford, International Journal of Fatigue, 23 (2001) S31 - S37.

[18] R..C. McClung, Fatigue and Fracture of Engineering Materials and Structures, 30 (2007) 173 - 205.

[19] S.B. Kim, A. Evans, J. Shackleton, G. Bruno, M. Preuss, P.J. Withers, Metallurgical and Materials Transactions A, 36A (2005) 3041 - 3053.

[20] J. Bergström, T. Ericsson, Surface Engineering, 2 (1986) 115 - 120.

[21] C. Bathias, J.P. Bonnafe, J.L. Lebrun, G. Maeder, X-Ray Diffraction and Acousitc Emission Study of Fatigue Damage in Aluminium Alloys, in: Champoux, Underwood, Kapp (Eds.) Analytical and Experimental Methods for Residual Stress Effects in Fatigue, ASTM STP 1004, ASTM, 1988, pp. 25 - 36.

[22] M.N. James, M. Newby, D.G. Hattingh, A. Steuwer, Procedia Engineering, 2 (2010) 441 - 451.

[23] T. Fujita, ISIJ International 32 (1992) 178-181.

[24] British Standard BS EN ISO 6507-1:2005 Metallic Materials - Vickers Hardness Test, Part 1: Test Method, 2005.

[25] British Standard BS EN 10002-1:2001 Metallic Materials - Tensile Testing, Part 1: Method of Test at Ambient Temperature, 2001.

[26] J.R. Davis, Stainless Steels, Second ed., ASM, 1994.

[27] British Standard BS EN ISO 4287:2000 Geometrical Product Specification (GPS) - Surface Texture: Profile Method - Terms, Definitions and Surface Texture Parameters, 2000.

[28] British Standard BS ISO 4288:1996 Geometric Product Specification (GPS) - Surface Texture - Profile Method: Rules and Procedures for the Assessment of Surface Texture, 1996.

[29] P.S. Prevéy, X-Ray Diffraction Residual Stress Techniques, in: ASM Handbook Volume 10, Materials Characterization, ASM, 1986, pp. 380 - 392.

[30] P.J. Withers, H.K.D.H. Bhadeshia, Materials Science and Technology, 17 (2001) 355 - 365.

[31] British Standard BS EN 15305:2008 Non-destructive Testing - Test Method for Residual Stress Analysis by X-ray Diffraction, 2008.

[32] M.E. Fitzpatrick, A.T. Fry, P. Holdway, F.A. Kandil, J. Shackleton, L. Suominen, Determination of Residual Stresses by X-Ray Diffraction, National Physical Laboratory, 2005.

[33] ESDU 92015, 1974.

[34] D. Novovic, R.C. Dewes, D.K. Aspinwall, W. Voice, P. Bowen, International Journal of Machine Tools and Manufacture, 44 (2004) 125 - 134.

[35] P.S. Maiya, D.E. Busch, Metallurgical Transactions A, 6A (1975) 1761 - 1766.

[36] P.S. Prevéy, in: Residual Stress for Designers and Metallurgists, ASM, Metals Park, Ohio, 1981, pp. 151 - 168.

[37] S.A. Martinez, S. Sathish, M.P. Blodgett, M.J. Shepard, Experimental Mechanics, 43 (2003) 141 - 147.

[38] H. Dölle, Journal of Applied Crystallography, 12 (1979) 489 - 501.

[39] M.G. Moore, W.P. Evans, SAE Transactions, 66 (1958) 340 - 345.

[40] D.J. Quesnel, M. Meshii, J.B. Cohen, Materials Science and Engineering 36 (1978) 207 - 215.

[41] J.F. Flavenot, N. Skalli, Effects of Grinding Conditions on Fatigue Behaviour of 42CD4 Grade Steel; Comparison of Different Fatigue Criteria Incorporating Residual Stresses, in: L. Mordfin (Ed.) Mechanical Relaxation of Residual Stresses, ASTM STP 993, ASTM, 1988, pp. 91 - 111.

[42] M.J. Balart, A. Bouzina, L. Edwards, M.E. Fitzpatrick, Materials Science and Engineering A, 367 (2004) 132 - 142.

[43] R.A. Poggie, J.J. Wert, Wear, 149 (1991) 209 - 220.

[44] S.A. Meguid, G. Shagal, J.C. Stranart, International Journal of Impact Engineering, 27 (2002) 119 - 134.

[45] J. Frankel, A. Abbate, W. Scholz, Experimental Mechanics, 33 (1993) 164 - 168.

[46] Z.H. Xu, X. Li, Acta Materialia, 53 (2005) 1913 - 1919.

# Figures and Captions

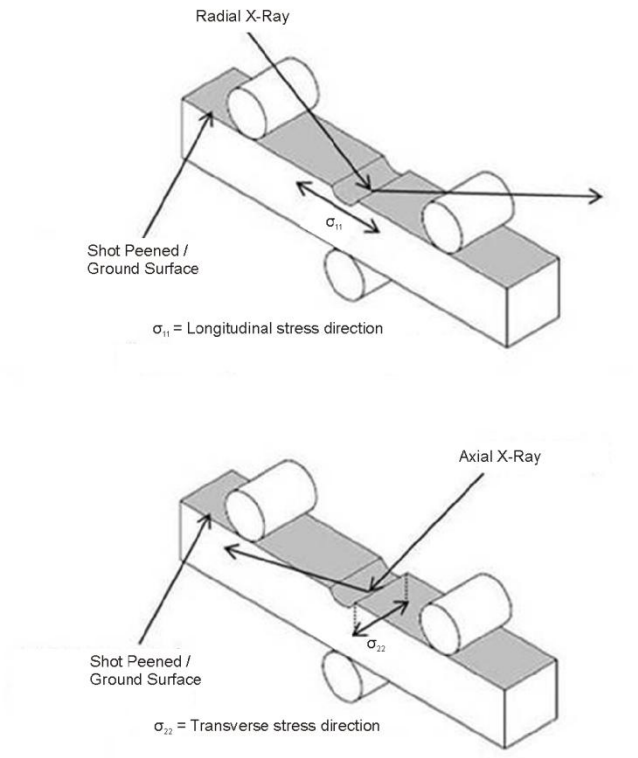


**Figure 1: X-Ray diffraction set up**

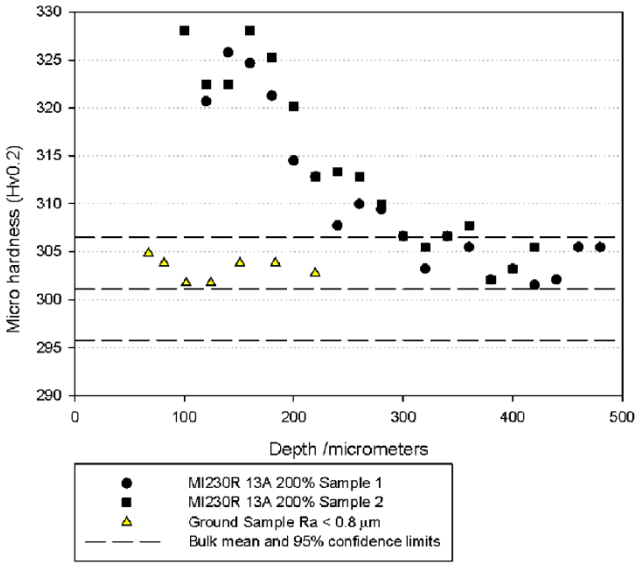


**Figure 2: Microhardness profiles after grinding and shot peening (T0) surface treatments**

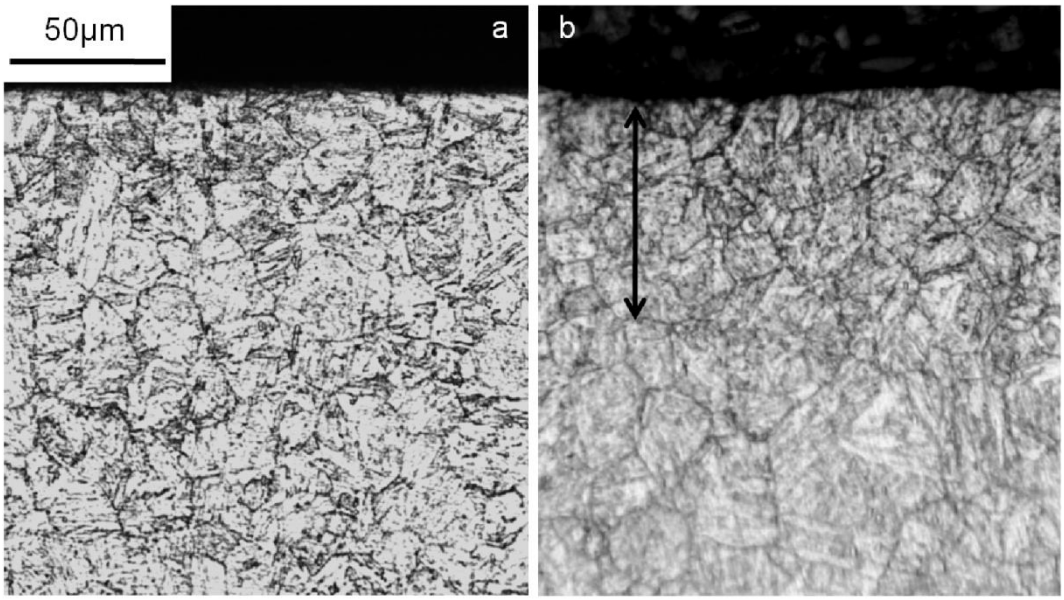


**Figure 3: Surface microstructure after a. grinding and b. shot peening (T0)**

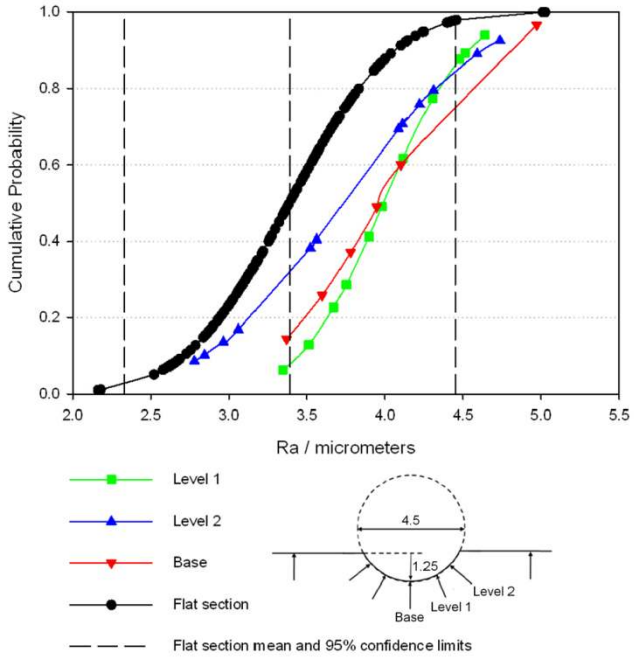


**Figure 4: Cumulative Ra probability (assuming normal density function for shot peened (T0) 4.5 x 1.25 mm notch**

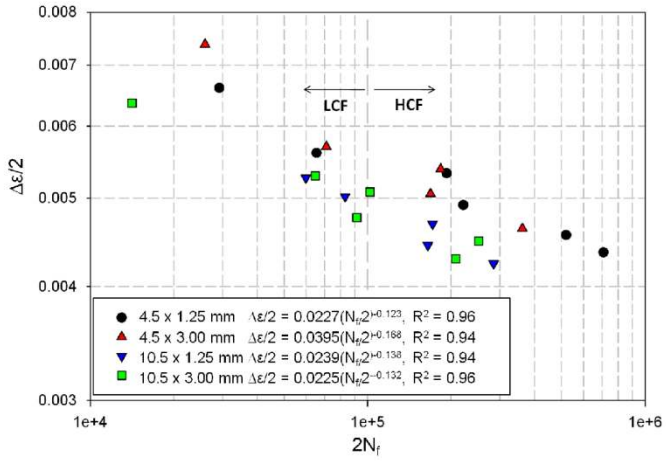


**Figure 5: Analogous Coffin Manson approach for shot peened (T0) notched samples of varying geometry**

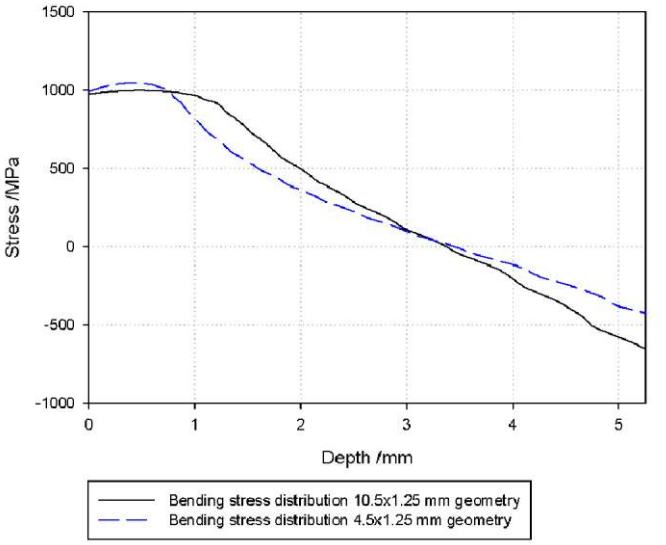


**Figure 6: Bending stress (longitudinal direction) in samples tested at strain range $10.5 \times 10^{-3}$ (determined using FE model)**

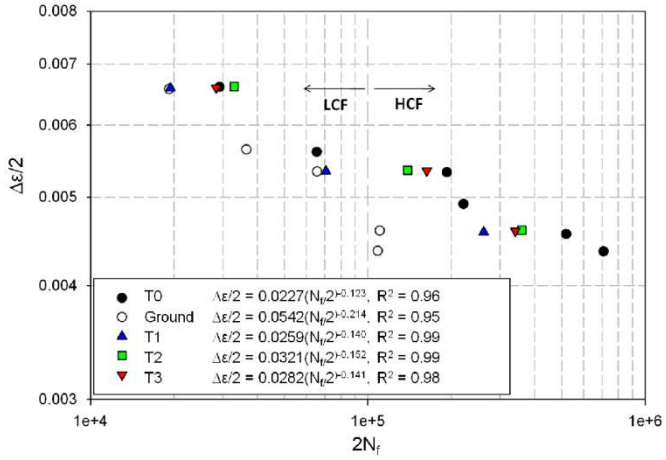


**Figure 7: Analogous Coffin Manson approach for notched samples (4.5 x 1.25 mm) after varying shot peening processes**

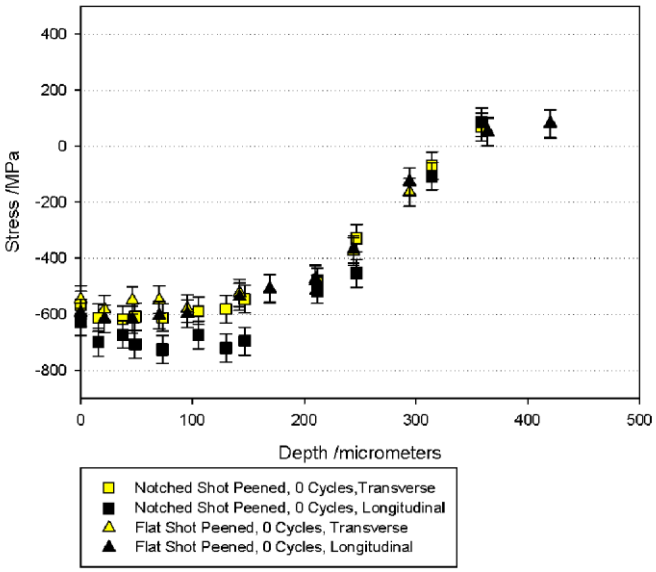


**Figure 8: Comparison of shot peened stress distributions in flat and notched samples**

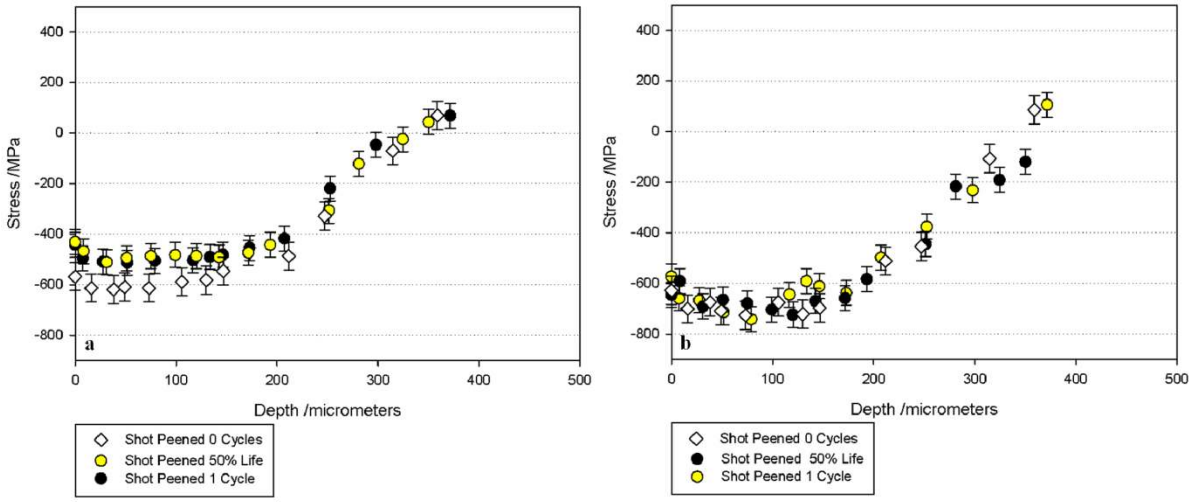


**Figure 9: Shot peening and post fatigue stresses in a. the transverse direction and b. the longitudinal direction**

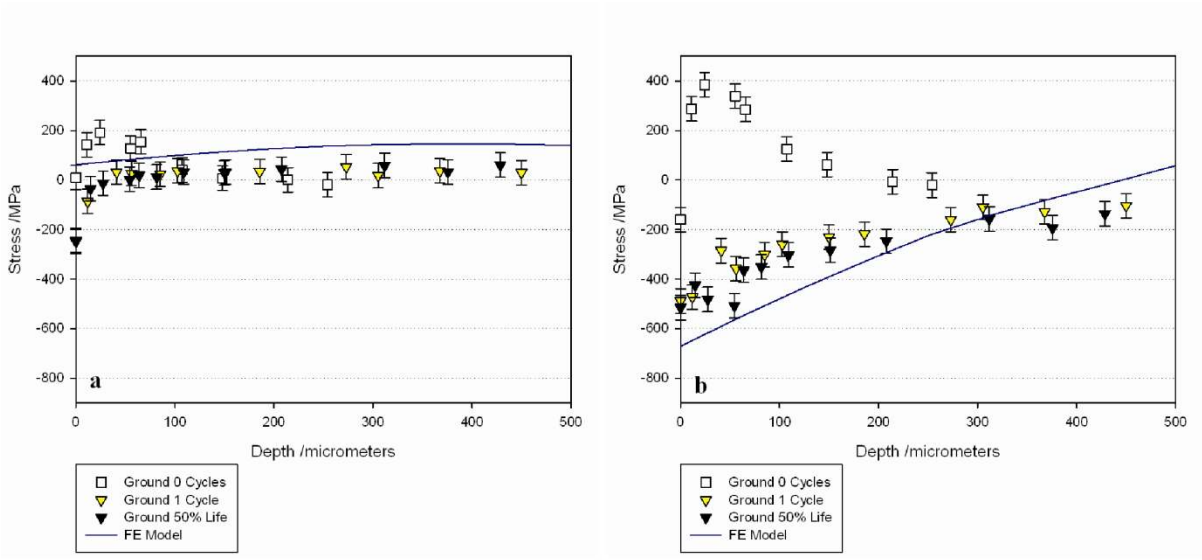


**Figure 10: Grinding and post fatigue stresses in a. the transverse direction and b. the longitudinal direction, also showing comparison with residual stresses predicted after one cycle by FE model**

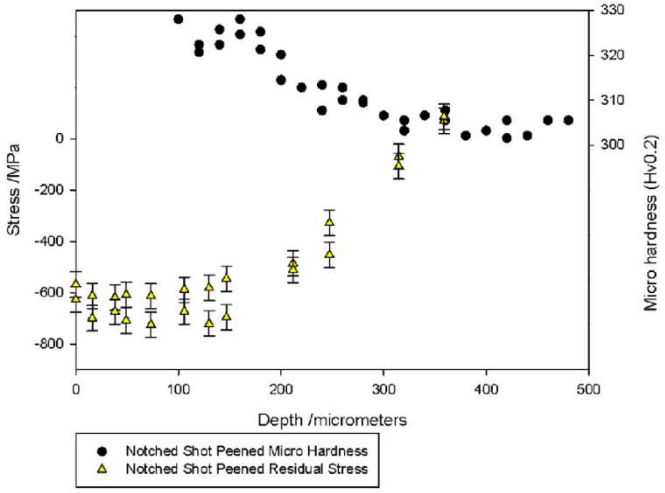


**Figure 11: Comparison of notched shot peened sample microhardness and residual stress profiles**

# Tables and Captions

| | C | Mn | Si | Ni | Cr | Mo | V | Nb | Fe | N |
|---|---|---|---|---|---|---|---|---|---|---|
| **FV448 nominal [23, 26]** | 0.13 | 1.0 | 0.5 | - | 10.5 | 0.75 | 0.15 | 0.45 | Bal | 0.05 |
| **FV448 (Spectrographic)** | 0.12 | 0.94 | 0.31 | 0.74 | 11.0 | 0.58 | 0.31 | 0.34 | Bal | - |

**Table 1: Composition of FV448 in wt%**

| | | Notch diameter / mm | |
|---|---|---|---|
| | | 4.5 | 10.5 |
| **Notch depth / mm** | 1.25 | Simulate blade connection geometry | Simulate repair like geometry |
| | 3.00 | Most severe service geometry | Complete test matrix |

**Table 2: Notch geometry variation**

| **Process** | **Intensity** | **Coverage /%** | **Shot diameter /mm** | **Shot hardness /HRC** | **Shot velocity /ms$^{-1}$** |
|---|---|---|---|---|---|
| MI110R 4A 200% (T1) | 4A | 200 | 0.28 | 45-52 | 26 |
| MI230R 13A 200% (T0) | 13A | 200 | 0.58 | 45-52 | 57 |
| MI330R 13A 200% (T2) | 13A | 200 | 0.84 | 45-52 | 35 |
| MI330R 18A 200% (T3) | 18A | 200 | 0.84 | 45-52 | 54 |

**Table 3: Shot peening process variation**

| **$H_{v10}$ /kgmm$^{-2}$** | **$H_{v0.2}$ /kgmm$^{-2}$** | **$\sigma_{0.2}$ /MPa** | **$\sigma_{uts}$ /MPa** | **% El at failure** |
|---|---|---|---|---|
| 312 ± 5 | 301 ± 5 | 806 ± 6 | 987 ± 9 | 12 ± 3 |
| **E /MPa** | **$\sigma_y$ /MPa** | **A** | **$n_m$** | |
| 201.3x10$^3$ | 806 | 1152 | 0.0587 | |

**Table 4: Hardness, monotonic tensile properties and corresponding material model data for FV448**

| **Surface Condition** | **$R_a$ / µm** | **95% Confidence Range** |
|---|---|---|
| Ground (parallel) | 0.029 | 0.011 |
| Ground (transverse) | 0.652 | 0.072 |
| T1 | 1.24 | 0.16 |
| T2 | 2.98 | 0.77 |
| T0 | 3.39 | 1.06 |
| T3 | 3.63 | 0.83 |

**Table 5: Surface roughness comparison for varying shot peening processes**